Acta Cryst. (1975). A31, 280

Unification of the Coincidence-Site-Lattice and Continuum Theories of Grain Boundaries*

BY M. J. MARCINKOWSKI† AND K. SADANANDA

Engineering Materials Group and Department of Mechanical Engineering, University of Maryland, College Park, Maryland 20742, *U.S.A.*

(*Received* 4 *September* 1974; *accepted* 20 *November* 1974)

The concepts embodied in the coincidence-site-lattice theory of grain boundaries are shown to be compatible with a large number of tensor quantities which have their origin in the continuum field theory of dislocations. More specifically such tensor quantities as distortion, grain-boundary dislocation density, and incompatibility have all been developed in terms of a general grain boundary for a continuum as well as for the discrete crystal. A generalized Burgers circuit about an arbitrary grain boundary is also shown to be a natural outcome of the present development.

Introduction

It was first shown that the plastic deformation of a grain boundary could be described in terms of a suitable combination of crystal lattice dislocations (CLD) from the two adjacent grains (Marcinkowski, 1970; 1972; Marcinkowski & Tseng, 1970; Das & Marcinkowski, 1971*a*; 1972; Sadananda & Marcinkowski, 1974*a*, *b*). Further development of this concept showed that the structure of the undeformed grain boundary itself could be described in terms of the same general concept involving the appropriate combination of CLD from the two adjacent grains (Marcinkowski & Das, 1972; Marcinkowski, Sadananda & Tseng, 1973; Marcinkowski & Sadananda, 1973; Marcinkowski & Dwarakadasa, 1973; Sadananda & Marcinkowski, 1973, 1974*c*). Not only was it found possible to integrate the theory of CLD into the present model of grain boundaries, but the theory of disclinations also followed quite logically (Das & Marcinkowski, 1971*b*; Marcinkowski, Das & Sadananda, 1973; Marcinkowski & Das, 1972). It was further shown that the present theory of grain boundaries could also be extended to arbitrary crystal structures (Marcinkowski, Tseng & Dwarakadasa, 1974; Tseng, Marcinkowski & Dwarakadasa, 1974). Because of these generalizations, the present theory of grain boundaries has been referred to as the unified theory.

Some very powerful mathematical techniques, based upon tensor algebra, have been developed over the years, which have led to marked insight into the behavior of dislocations (Kröner, 1958) as well as disclinations (de Wit, 1970). The purpose of the present study has been to extend these mathematical methods to grain boundaries in order to form the basis of a still more generalized and unified theory of grain boundaries.

* The present research effort was supported by The National Science Foundation under Grant No. GH-32262.

† Presently on sabbatical leave at the Institut für Theoretische und Angewandte Physik der Universität Stuttgart, Germany (BRD).

Plastic distortions which give rise to rigid rotations

Fig. 1(*a*) shows a block of material which may be visualized as a single crystal or grain. On may now define a plastic distortion $\mathbf{D}=D_{ij}$ which is expressed by the following relation:

$$D_{ij}=\Delta u_i/\Delta x_j \tag{1}$$

where Δu_i is the relative displacement between two parallel planes originally separated by a distance Δx_j. For small displacements, equation (1) is more usually written as e_{ij} (Nye, 1957), while Kröner (1958) expresses his distortion as $\beta_{ji}=D_{ij}$. Fig. 1(*c*) may be visualized as being derived from Fig. 1(*a*) by carrying out the specific distortion

$$D^1_{ij}=\begin{pmatrix}D_{11}D_{12}D_{13}\\D_{21}D_{22}D_{23}\\D_{31}D_{32}D_{33}\end{pmatrix}=\begin{pmatrix}0 & \tan\theta/2 & 0\\0 & 0 & 0\\0 & 0 & 0\end{pmatrix} \tag{2}$$

which is equivalent to a simple shear. In the case where D_{ij} possesses a limiting value, *i.e.*

$$\lim_{\Delta x_j\to 0}=\frac{\Delta u_i}{\Delta x_j}=\frac{\mathrm{d}u_i}{\mathrm{d}x_j} \tag{3}$$

the distortion shown in Fig. 1(*b*) obtains, and D_{ij} may be written as

$$D_{ij}=\partial u_i/\partial x_j\equiv\partial_j u_i\equiv u_{i,j}\,. \tag{4}$$

The distortion shown in Fig. 1(*b*) may be referred to as the type given in the continuum model, while that shown in Fig. 1(*c*) may be thought of as that expressed by the discrete model. Note that the distortions in Fig. 1 result in no net rotation of the crystal.

It is next of interest to investigate the strain tensor E_{ij} associated with a given finite distortion D_{ij}. According to Duschek & Hochrainer (1960)

$$E_{ij}=\tfrac{1}{2}(D_{ij}+D_{ji}+D_{ki}D_{kj}) \tag{5}$$

where E_{ij} is referred to as the strain tensor in Lagrangian coordinates, *i.e.* coordinates prior to deformation (Fung, 1965). The **E** associated with the distortion

given by equation (2) may then be readily expressed by

$$E^1_{ij}=\begin{pmatrix}E_{11}E_{12}E_{13}\\E_{21}E_{22}E_{23}\\E_{31}E_{32}E_{33}\end{pmatrix}=\begin{pmatrix}0 & \frac{1}{2}\tan\theta/2 & 0\\ \frac{1}{2}\tan\theta/2 & \frac{1}{2}\tan^2\theta/2 & 0\\ 0 & 0 & 0\end{pmatrix}. \quad (6)$$

In general there is no simple physical interpretation associated with the components of the strain tensor resulting from large distortions. However, E_{ij} given by equation (5) can be used to determine the volume

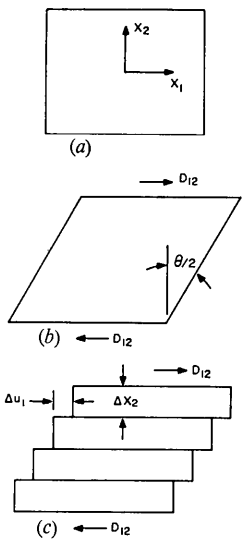

Fig. 1. Simple shear of the single grain shown in (*a*) by (*b*) continuous (*c*) discrete slip motion.

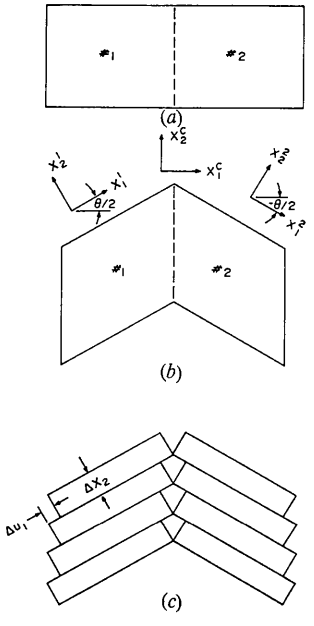

Fig. 2. Generation of a symmetric tilt boundary from the single grain shown in (*a*) by (*b*) continuous (*c*) discrete slip motion.

change Δ associated with the particular distortion. In particular, according to Duschek & Hochrainer (1960).

$$\Delta=(V-V_0)/V_0=[\det(\delta_{ij}+2E_{ij})]^{1/2}-1\,, \quad (7)$$

where V_0 and V are the volumes prior to and after plastic distortion respectively, while det signifies the determinant of the quantity in parentheses. The symbol δ_{ij} refers to the Kronecker delta (Flügge, 1972). For the particular case of equation (6), Δ from equation (7) is readily found to be zero as is physically anticipated from inspection of Fig. 1. As later discussions will indicate, the nature of the volume change associated with a given distortion is not always physically obvious.

Fig. 2(*a*) again shows a block of material which may be viewed as a single crystal. This time however, the block can be subdivided into two distinct regions labeled as #1 and #2 and separated by the vertical dashed line. One may now carry out the distortions D^1_{ij} given by equation (2) and $D^2_{ij}=-D^1_{ij}$ within regions #1 and #2 respectively. The resulting distortion is shown in Fig. 2(*b*) and (*c*), where the former is in terms of the continuum model, while the latter is in terms of the discrete representation. It is apparent that the combined distortions D^1_{ij} and D^2_{ij} have resulted in the counterclockwise and clockwise rotations of grains #1 and #2 respectively by $\theta/2$ measured with respect to the original coordinate system designated by the superscript *c*. The net result has been the creation of a grain boundary between grains #1 and #2.

In the case of twist boundaries or a completely enclosed symmetric tilt boundary, it is necessary to generalize the distortion given by equation (2) as follows:

$$D^{1'}_{ij}=\begin{pmatrix}0 & \tan\theta/2 & 0\\ -\tan\theta/2 & 0 & 0\\ 0 & 0 & 0\end{pmatrix}. \quad (8)$$

From equation (5), the strain tensor associated with the above distortion is found to be

$$E^{1'}_{ij}=\begin{pmatrix}\frac{1}{2}\tan^2\theta/2 & 0 & 0\\ 0 & \frac{1}{2}\tan^2\theta/2 & 0\\ 0 & 0 & 0\end{pmatrix}. \quad (9)$$

The above strain leads in turn to a volume change, which from equation (7), is found to be

$$\Delta=\tan^2\theta/2\,. \quad (10)$$

The nature of this volume change can be visualized by reference to Fig. 3(*b*) which arises from the application of the distortion given by equation (8) to the single grain shown in Fig. 3(*a*), which may be thought of as grain #1. For visualization purposes, the model shown in Fig. 3(*b*) is best taken as discrete. Furthermore, θ is chosen as 53·1°, which later sections will show corresponds to a coincidence lattice orientation. For this particular value of θ, equation (10) leads to a volume change given by $\Delta=0{\cdot}25$. This volume change is represented by the shaded areas in Fig. 3(*b*), and each one of these areas may be associated with a pair of

dislocation dipoles, *i.e.* a row of vacancies lying along the x_3^c axis. Several of these dislocations are shown in the upper right-hand corner of the figure, and it is a simple matter to show that the sum of all the Burgers vectors associated with Fig. 3(*b*) is zero. Another way of looking at this figure is to visualize all of the dislocations as originating from loops, or plus–minus edge-type pairs, during the distortion given by equation (8). Distortions similar to that shown in Fig. 3(*b*) have also been postulated by Cottrell (1957) but in a somewhat different context.

In order to eliminate the excess volume, *i.e.* excess vacancies in Fig. 3(*b*), and thus maintain a low-energy grain boundary, it is necessary to superimpose a volume distortion D_{ij}^{1V} on Fig. 3(*b*) such that $\Delta=0$, as shown in this figure. The distortion can then be written as

$$D_{ij}^{1''}=D_{ij}^{1'}+D_{ij}^{1V} \tag{11}$$

where $D_{ij}^{1'}$ is given by equation (8) and D_{ij}^{1V} is expressed by the following:

$$D_{ij}^{1'V}=\begin{pmatrix} D_{11}^{1V} & 0 & 0 \\ 0 & D_{22}^{1V} & 0 \\ 0 & 0 & 0 \end{pmatrix}. \tag{12}$$

As $D_{11}^{1V}=D_{22}^{1V}$ in the above equation, equation (5) can be used to obtain the corresponding strain tensor

$$E_{ij}^{1V}=\begin{pmatrix} D_{11}^{1V}+\frac{1}{2}(D_{11}^{1V})^2 & 0 & 0 \\ 0 & D_{11}^{1V}+\frac{1}{2}(D_{11}^{1V})^2 & 0 \\ 0 & 0 & 0 \end{pmatrix}. \tag{13}$$

The above relation can then be used to obtain the corresponding volume change through equation (7), *i.e.*

$$\Delta=(D_{11}^{1V})^2+2D_{11}^{1V}. \tag{14}$$

Since Δ given by the above equation must be equal to the negative of that given by relation (10), we obtain

$$D_{11}^{1V}=-1\pm\sqrt{1-\tan^2\theta/2} \tag{15}$$

where the positive root is used. The above analysis applied to grain #1 in Fig. 3, could also be carried out for the surrounding matrix, *i.e.* grain #2. Analogous to the case described in Fig. 2, the combined distortions of grains #1 and #2 in Fig. 3 lead to their mutual rigid rotation by $\theta/2$ with respect to the original *c* coordinate system. The rotation of one such grain, *i.e.* grain #1, by $\theta/2$ is shown in Fig. 3(*d*). For convenience, the distortions illustrated in Fig. 3(*c*) and (*d*) are based upon the continuum model, in contrast to those of Fig. 3(*a*) and 3(*b*).

The distortions associated with Figs. 1, 2 and 3 have all been described in terms of glide motions. On the other hand, it is possible to generate the same net distortion by a climb process which involves atom diffusion. Such a process is shown in Fig. 4 where the block designated by *ABCD* is converted into that described by *AEFD*. In particular, the vertical planes describing the section *ABE* drawn dotted climb upward as shown by the arrow, while those planes contained in *DCF* occur as a result of downward climb. The final distortion is identical to that given in Fig. 1(*b*). It thus follows that a history is associated with the formation of a grain boundary. On the other hand, the distortion associated with Fig. 4 is still formally the same as that given by equation (2).

In concluding this section, it is to be emphasized that the plastic distortions described thus far refer only to the distortions within the individual grains. Although these distortions give the correct angular

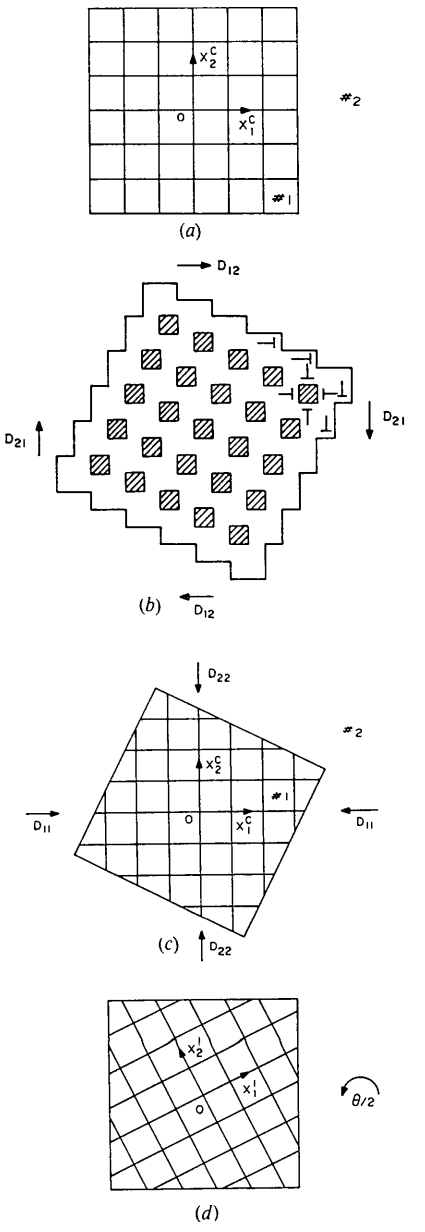

Fig. 3. (*b*) Plastic distortion of the single grain shown in (*a*) by glide on two orthogonal slip systems. Discrete approximation. (*c*) Hydrostatic compression of the grain shown in (*b*) followed by a counterclockwise rotation shown in (*d*). Continuum approximation.

rotations associated with the boundaries through the distortion components $\tan\theta/2$, they do not in themselves properly describe the plastic distortion associated with a pure rigid-body rotation. This aspect of the problem will now be considered in more detail in the following section.

Generalized formulation of symmetric boundaries

In general, a rigid-body rotation through an angle φ can be described in terms of the generalized rotation tensor R_{ij} given by (Duschek & Hochrainer, 1960)

$$R_{ij}=e_ie_j+(\delta_{ij}-e_ie_j)\cos\varphi+\varepsilon_{ijk}e_k\sin\varphi \qquad (16)$$

where e_i is a unit vector in the direction of the rotation axis. The quantity ε_{ijk} in equation (16) is the permutation tensor (Flügge, 1972). The rotation tensor given by equation (16) can then be used to relate the coordinates in the two corresponding systems according to (Nye, 1957)

$$x_i'=R_{ij}x_j \qquad (17a)$$

or

$$x_i=R_{ji}x_j' \qquad (17b)$$

where the primes refer to the coordinates in the rotated system, while the unprimed quantities refer to the coordinates in the original unrotated system. If equations (17) are applied to Fig. 2, it follows that

$$x_i^1=R_{ij}^{1c}x_j^c \qquad (18a)$$

or

$$x_i^c=R_{ij}^{1c}x_j^1 \qquad (18b)$$

while

$$x_i^2=R_{ij}^{2c}x_j^c \qquad (19a)$$

or

$$x_i^c=R_{ji}^{2c}x_j^2\,, \qquad (19b)$$

where from equation (16), in which the rotation axis is chosen to lie along z,

$$R_{ij}^{1c}=\begin{pmatrix}\cos\theta/2 & \sin\theta/2 & 0\\ -\sin\theta/2 & \cos\theta/2 & 0\\ 0 & 0 & 1\end{pmatrix} \qquad (20a)$$

while

$$R_{ij}^{2c}=R_{ji}^{1c}. \qquad (20b)$$

Equations (18) also apply to Fig. 3. It is also apparent that the coordinates of grains #1 and #2 in Fig. 2 can also be related to one another through equations (18) and (19) to give

$$x_i^1=R_{ij}^{1c}R_{kj}^{2c}x_k^2=R_{ik}^{12}x_k^2 \qquad (21a)$$

or

$$x_i^1=R_{ki}^{12}x_k^2 \qquad (21b)$$

where

$$R_{ik}^{12}=\begin{pmatrix}\cos\theta & \sin\theta & 0\\ -\sin\theta & \cos\theta & 0\\ 0 & 0 & 1\end{pmatrix}. \qquad (22)$$

Equations (21) and (22) will again be taken up in the discussion of asymmetric tilt boundaries.

A displacement vector u_i can be associated with a rotation as follows (Duschek & Hochrainer):

$$u_i=x_i'-x_i=(R_{ij}-\delta_{ij})x_j \qquad (23)$$

where equation (17a) has been utilized in arriving at the above relations. A distortion tensor associated with a rigid-body rotation may now be defined as the term in parentheses in equation (23), *i.e.*

$$D_{ij}^R=R_{ij}-\delta_{ij}\,. \qquad (24)$$

With respect to Fig. 2(b), the distortion tensor D_{ij}^R can be defined separately for grains #1 and #2 in terms of the c coordinate system. In particular

$$u_i^{1,c}=x_i^1-x_i^c=D_{ij}^{1c}x_j^c \qquad (25a)$$

and

$$u_i^{2,c}=x_i^2-x_i^c=D_{ij}^{2c}x_j^c \qquad (25b)$$

where

$$D_{ij}^{1c}=R_{ij}^{1c}-\delta_{ij} \qquad (26a)$$

and

$$D_{ij}^{2c}=R_{ij}^{2c}-\delta_{ij}\,. \qquad (26b)$$

Alternatively, equations (25) and (26) can be combined to give the distortion relating to both grains #1 and #2 of Fig. 2(b). In particular

$$u_i^{1,2,c}=u_i^{1,c}-u_i^{2,c}=D_{ij}^{1,2,c}x_j^c \qquad (27a)$$

where from equation (26)

$$D_{ij}^{1,2,c}=R_{ij}^{1c}-R_{ij}^{2c}=D_{ij}^{1c}-D_{ij}^{2c}. \qquad (27b)$$

With the aid of equations (20), (26) and (27) D_{ij}^{1c} and $D_{ij}^{1,2,c}$ can be written out in full as

$$D_{ij}^{1c}=\begin{pmatrix}\cos\theta/2-1 & \sin\theta/2 & 0\\ -\sin\theta/2 & \cos\theta/2-1 & 0\\ 0 & 0 & 0\end{pmatrix} \qquad (28a)$$

while

$$D_{ij}^{1,2,c}=\begin{pmatrix}0 & 2\sin\theta/2 & 0\\ -2\sin\theta/2 & 0 & 0\\ 0 & 0 & 0\end{pmatrix} \qquad (28b)$$

where it is immediately apparent that $D_{ij}^{1,2,c}$ is antisymmetric, *i.e.* $D_{ij}^{1,2,c}=-D_{ji}^{1,2,c}$. As expected for a rigid-body rotation, equation (28a), through the use of equations (5) and (7), leads to E_{ij}^{1c} and Δ both equal to zero. On the other hand, equations (5) and (7) are, strictly speaking, not applicable to $D_{ij}^{1,2,c}$ since the

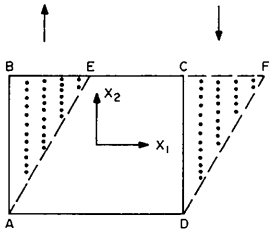

Fig. 4. Distortion of the block *ABCD* into *AEFD* by climb processes.

components of this particular tensor apply to a surface, *i.e.* the grain boundary separating grains $\#1$ and $\#2$ from one another.

Still more insight into the significance of equations (28*a*) and (28*b*) can be obtained by reference to Fig. 5 which shows the displacements and distortions associated with a grain boundary possessing an orientation similar to that shown in Fig. 2(*b*). With the aid of equations (25), (26), (27) and (28), it is apparent from this figure that $x_2^1 \equiv OA$, $x_2^c \equiv OD$, $x_2^2 \equiv OB$, $CA \equiv u_1^{1,c} = D_{12}^{1,c} x_2^c$, $CB \equiv u_1^{2,c} = D_{12}^{2,c} x_2^c$ and $u_2^{1,c} = D_{22}^{1,c} x_2^c = D_{22}^{2,c} x_2^c = u_2^{2,c} = CD$. Thus it can be seen from equation (27*b*) how the diagonal elements of $D_{ij}^{1,2,c}$, which are related to CD in Fig. 5, cancel. On the other hand, the non-diagonal element $D_{12}^{1,2,c}$ in equation (28*b*) is simply the ratio AB/OD, or since $OD = OA$, AB/OA. It will be shown in a subsequent section that $D_{12}^{1,2,c}$ is simply the dislocation density along a symmetric boundary in the x_2^c direction, while $D_{21}^{1,2,c}$ is the dislocation density along the corresponding grain boundary in the x_1^c direction.

Special case of low-angle boundaries

As θ approaches zero, equations (26) and (28) reduce to the following:

$$D_{ij}^{1,2,c} = \begin{pmatrix} 0 & \theta & 0 \\ -\theta & 0 & 0 \\ 0 & 0 & 0 \end{pmatrix} \tag{29a}$$

and

$$D_{ij}^{1,c} = \begin{pmatrix} 0 & \theta/2 & 0 \\ -\theta/2 & 0 & 0 \\ 0 & 0 & 0 \end{pmatrix}. \tag{29b}$$

Unlike the case for large angles, in which only $D_{ij}^{1,2,c}$ was antisymmetric, $D_{ij}^{1,c}$ and $D_{ij}^{2,c}$ are also antisymmetric for small θ. Furthermore, since θ is small, the product term in equation (5) can be neglected, so that

$$E_{ij} = \tfrac{1}{2}(D_{ij} + D_{ji}) = \tfrac{1}{2}(\partial_j u_i + \partial_i u_j) \tag{30}$$

where it is apparent that all E_{ij} associated with equations (29) are zero. Since the distortion tensors given by equations (29) are antisymmetric, since for small strains

$$\Delta = E_{ii} = 0 \tag{31}$$

it follows that they represent pure rotations. They can thus be written as (Nye, 1957)

$$D_{ij} \equiv \omega_{ij} = \tfrac{1}{2}(\partial_j u_i - \partial_i u_j) \tag{32}$$

or in vector form as (Kröner, 1966)

$$\left.\begin{aligned} \boldsymbol{\omega} &= \tfrac{1}{2} \operatorname{curl} \mathbf{u} \\ \omega_k &= \tfrac{1}{2}\varepsilon_{kij}\omega_{ij} = \tfrac{1}{2}\varepsilon_{kij}\partial_j u_i \end{aligned}\right\} \tag{33a}$$

or conversely as

$$\omega_{ij} = \varepsilon_{ijk}\omega_k \,. \tag{33b}$$

It is important to emphasize here that equations (32) and (33) hold in general only for small θ. Also in accordance with the discussion at the end of the previous section, it is apparent that the components of the tensors in equations (29) represent the dislocation densities for low-angle tilt boundaries.

Grain-boundary dislocation density

Although we have already touched on the meaning of a grain-boundary dislocation density, it is instructive to approach this subject from a somewhat different point of view. In particular, the dislocation density within a grain boundary may be expressed by (Kröner, 1958; Bilby, 1955)

$$\left.\begin{aligned} \bar{\boldsymbol{\alpha}} &= \mathbf{n} \times \mathbf{D}|_{\#2} - \mathbf{n} \times \mathbf{D}|_{\#1} \\ -\bar{\alpha}_{ij} &= \varepsilon_{ikl} n_k D_{jl}|_{\#2} - \varepsilon_{ikl} n_k D_{jl}|_{\#1} \end{aligned}\right\} \tag{34}$$

where $\mathbf{D}$ is the plastic distortion tensor, $\mathbf{n}$ is a unit vector normal to the grain boundary directed from grain $\#1$ to grain $\#2$, while the indices i and j refer to the plane normal (or dislocation line direction in the present case) and Burgers vector component associated with $\bar{\boldsymbol{\alpha}}$. The subscripts $\#2$ and $\#1$ signify that the operations associated with those particular terms are defined with respect to grains $\#2$ and $\#1$ respectively. As an example, for the symmetric tilt boundary shown in Fig. 2, $\bar{\boldsymbol{\alpha}}$ is given by

$$-\bar{\alpha}_{31} = \varepsilon_{312} n_1 D_{12}^{2,c}|_{\#2} - \varepsilon_{312} n_1 D_{12}^{1,c}|_{\#1} \tag{35a}$$

$$-\bar{\alpha}_{31} = -\sin\theta/2|_{\#2} - \sin\theta/2|_{\#1} \tag{35b}$$

$$\bar{\alpha}_{31} = 2\sin\theta/2 \,. \tag{35c}$$

On the other hand

$$-\bar{\alpha}_{32} = \varepsilon_{312} n_1 D_{22}^{2,c}|_{\#2} - \varepsilon_{312} n_1 D_{22}^{1,c}|_{\#1} \tag{36a}$$

$$-\bar{\alpha}_{32} = (\cos\theta/2 - 1)|_{\#2} - (\cos\theta/|2 - 1)_{\#1} \tag{36b}$$

$$\bar{\alpha}_{32} = 0 \,, \tag{36c}$$

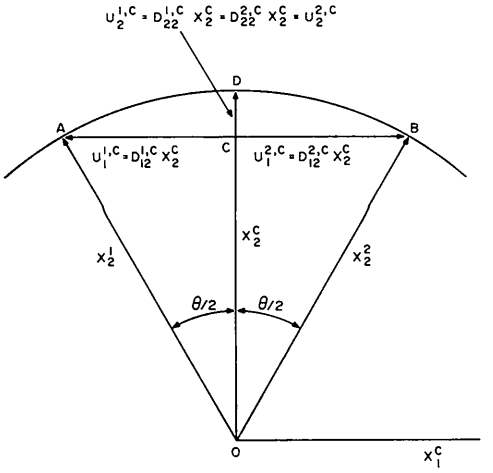

Fig. 5. Schematic illustration of the distortion associated with a rigid-body rotation.

where it is apparent that the value of n_1 in the above equations is unity, while the plastic distortions given by equations (26) and (28*a*) have been used. It is also apparent that the grain-boundary dislocation density components α_{31} and α_{32}, given by equations (35) and (36), are simply the components of the distortion tensor $D_{ij}^{1,2,c}$ given by $D_{12}^{1,2,c}$ and $D_{22}^{1,2,c}$ respectively.

Yet another way of expressing $\bar{\boldsymbol{\alpha}}$ is in terms of the distortions D_{ij}^1 and D_{ij}^2 within the individual grains given by equation (2). In this case, equation (34) becomes

$$-\bar{\alpha}_{31}=\varepsilon_{312}n_1D_{12}^2|_{\neq 2}-\varepsilon_{312}n_1D_{12}^1|_{\neq 1} \tag{37a}$$

$$-\bar{\alpha}_{31}=\cos\theta/2(-\tan\theta/2)|_{\neq 2}-\cos\theta/2(\tan\theta/2)|_{\neq 1} \tag{37b}$$

$$-\bar{\alpha}_{31}=2\cos\theta/2\tan\theta/2=2\sin\theta/2 \tag{37c}$$

which is seen to be identical to the results given by equations (35). It is important to note that in using equation (37) **n** has been chosen normal to the deformed face of Fig. 1(*b*).

It can also be seen that as $\theta\to 0$, equations (34), (32) and (33*b*) can be combined to give

$$\bar{\alpha}_{ij}=(\delta_{ij}n_m\omega_m^{2,c}-n_j\omega_i^{2,c})_{\neq 2}-(\delta_{ij}n_m\omega_m^{1,c}-n_j\omega_i^{1,c})|_{\neq 1}\,. \tag{38}$$

The individual terms in the above expression are related to the lattice curvatures (Kröner, 1958). In comparison with the case for large θ given by equations (35), equation (38) gives

$$\bar{\alpha}_{31}=-n_1\omega_3^{1,2}|_{\neq 2}+n_1\omega_3^{1,2}=\theta/2+\theta/2=\theta \tag{39}$$

as expected, and is thus in accord with the value of the $D_{12}^{1,2,c}$ component of the distortion tensor given by equation (29*a*).

Asymmetric tilt boundaries and grain-boundary incompatibility

Fig. 6(*a*) shows the particular case of a grain boundary which has been formed by first subjecting grain #1 in Fig. 2(*a*) to a plastic distortion given by $D_{12}^1=\tan\theta$, with all other components zero. Such a distortion

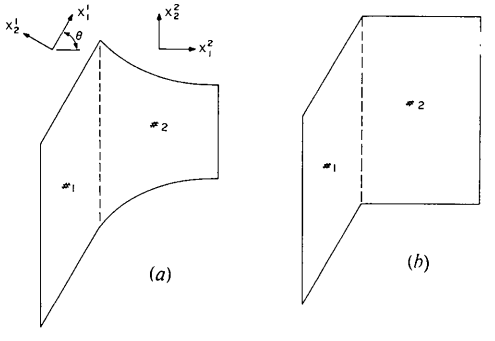

Fig. 6. Generation of an asymmetric tilt boundary from the single grain shown in Fig. 2(*a*) by continuous slip motion (*a*), after rotation of grain #1(*b*), after dilatation of grain #2.

induces a counterclockwise rotation of grain #1 with respect to grain #2 in the manner given by equation (22). The displacement vectors associated with this distortion are seen to be

$$u_i^{1,2}=x_i^1-x_i^2=D_{ij}^{1,2}x_i^2 \tag{40}$$

where

$$D_{ij}^{1,2}=R_{ij}^{1,2}-\delta_{ij}\,. \tag{41}$$

From equation (34) the grain boundary dislocation density contributed from grain #1 is given by $\bar{\alpha}_{31}=\sin\theta$ and $\bar{\alpha}_{32}=\cos\theta-1$. On the other hand, since $\mathbf{D}^2$ associated with grain #2 is zero, there exists no $\bar{\alpha}$ contribution from it. However, in order for grains #1 and #2 to retain their coherency across the grain boundary during the plastic deformation within grain #1, severe elastic strains must be generated within grains #1 and #2. This is shown by the curved upper and lower surfaces of grain #2 in Fig. 6(*a*).

As a measure of the elastic distortions exhibited in Fig. 6(*a*), it is helpful to introduce the concept of an incompatibility tensor **H** defined as follows (Kröner, 1958):

$$\mathbf{H}=-\nabla\times\mathbf{D}\times\nabla \tag{42a}$$

or alternatively as

$$\left.\begin{aligned}\mathbf{H}&=\bar{\boldsymbol{\alpha}}\times\nabla\\ H_{il}&=\varepsilon_{ijk}\nabla_k\bar{\alpha}_{lj}\end{aligned}\right\}. \tag{42b}$$

The tensor **H** may be visualized as a measure of the internal elastic strain existing within a body. In the case of Fig. 6(*a*) **H** may be written as

$$H_{il}^{1,2}=\begin{pmatrix}0&0&0\\0&0&0\\0&0&H_{33}^{1,2}\end{pmatrix} \tag{43}$$

where

$$H_{33}^{1,2}=\varepsilon_{312}\nabla_2\bar{\alpha}_{31}+\varepsilon_{321}\nabla_1\bar{\alpha}_{32} \tag{44a}$$

$$H_{33}^{1,2}=0-\partial/\partial x[\cos\theta-1]\neq 0\,. \tag{44b}$$

It is apparent from equation (44*b*) that the incompatibility associated with the grain boundary in Fig. 6(*a*) arises because of the component $H_{33}^{1,2}$. This incompatibility however can be removed by subjecting grain #2 in Fig. 6(*a*) to the distortion

$$D_{22}^2=(\cos\theta-1)\,. \tag{45}$$

This enables α_{32} and thus the component $H_{33}^{1,2}$ to vanish. The effects of the distortion given by equation (45) are shown in Fig. 6(*b*) and can be visualized as being obtained by the insertion of crystal lattice dislocations of density $\bar{\alpha}_{32}=\cos\theta-1$ into grain #2 of Fig. 6(*a*). The terms compensated and uncompensated grain boundaries have been employed to describe the configurations shown in Fig. 6(*b*) and 6(*a*) respectively (Marcinkowski & Sadananda, 1973). It is easy to see that the incompatibility **H** also vanishes for the case of the symmetric tilt boundary shown in Fig. 2. On the other hand, as $\theta\to 0$, $\bar{\alpha}_{32}\to 0$ for the case shown in Fig. 6, *i.e.* the asymmetric tilt boundary becomes symme-

tric, so that **H** for this particular boundary also vanishes.

Relationship between the continuum theory and the coincidence-site theory of grain boundaries

A more detailed atomistic picture of the symmetric tilt boundary discussed with respect to Fig. 2(*b*) is shown in Fig. 7. For simplicity, the crystal structure is taken to be simple cubic, θ is 53·1° and the rotation axis is taken to be normal to the drawing, *i.e.* [001]. A characteristic feature of the grain boundary in Fig. 7 is that it possesses a common lattice or unit cell. Two such unit cells, one in each grain, are shown in heavy outline and are seen to be coincident with the coordinate system labeled with the superscript *c*. One of the coincidence-site-lattice unit cells of Fig. 7 is shown in still greater detail in Fig. 8.

The coincidence-site-lattice relationship has been defined in earlier studies by the following relationship (Marcinkowski & Das, 1972; Marcinkowski, Sadananda & Tseng, 1973):

$$\tan\theta/2=\frac{Nb}{Mb}=\frac{N}{M} \tag{46}$$

where N has been visualized as the number of crystal lattice dislocations of strength b, shown in heavy outline within the grain boundary of Fig. 7, which have moved to the grain boundary from either grain #1 or grain #2 on every M successive slip planes. The quantities N and M may possess any integer value, and it is clear that the unit-cell demensions of the coincidence-site lattice a_{0c} are defined by this pair of integers as follows

$$a_{0c}=a_0(N^2+M^2)^{1/2}. \tag{47}$$

For the particular case where $\theta=53{\cdot}1°$ shown in Fig. 7, $N=1$ and $M=2$ as can be seen in Fig. 8. It is also clear from equations (2) and (8) of the previous discussions that the coincidence-site-lattice relationship given by equation (46) is simply one of the components of the distortion tensor referred to one of the grains, *i.e.* D^1_{12} or D^2_{12}.

In order that the dislocation content associated with an asymmetric grain boundary in a discrete crystal lattice be visualized, reference is made to Fig. 9. Specifically, as in the case of Fig. 7, the grain boundary in Fig. 9 possesses a tilt angle of 53·1°; however the boundary is rotated from its symmetric orientation by $\varphi=$ 26·6°. The detailed dislocation structure comprising the straight asymmetric tilt boundary, unlike the continuum model of Fig. 6(*b*), is readily discernible in Fig. 9. For example, two crystal-lattice dislocations are seen to occur at the grain boundary every five interatomic spacings along the x_2^2 direction of grain #2. This corresponds to $\bar{\alpha}_{32}=\frac{2}{5}=0{\cdot}40$, which is in agreement with the value $\bar{\alpha}_{32}=\cos(53{\cdot}1)-1=0{\cdot}40$ obtained from equation (36).

The asymmetric tilt boundary shown in Fig. 9 can also be visualized in terms of a stepped boundary such as illustrated in Fig. 10 (Marcinkowski & Sadananda, 1973) where each stepped segment consists of a symmetric tilt boundary. It is also apparent from comparison of Figs. 9 and 10 that the dislocation content within each of the grain boundaries is markedly different. The difference may be understood by visualizing Fig. 9 as being formed by a rotation of grain #1 by θ with respect to grain #2, *i.e.* by equations (40) and (41). The stepped asymmetric boundary in Fig. 10, on the other hand, may be viewed in terms of equal but opposite rotations of grains #1 and #2 by angles of $\theta/2$, *i.e.* by equations (25) and (26). Unique coincidence-site lattices are also possessed by the asymmetric tilt boundaries of Figs. 9 and 10 and they have been discussed in detail elsewhere (Marcinkowski & Sadananda, 1973).

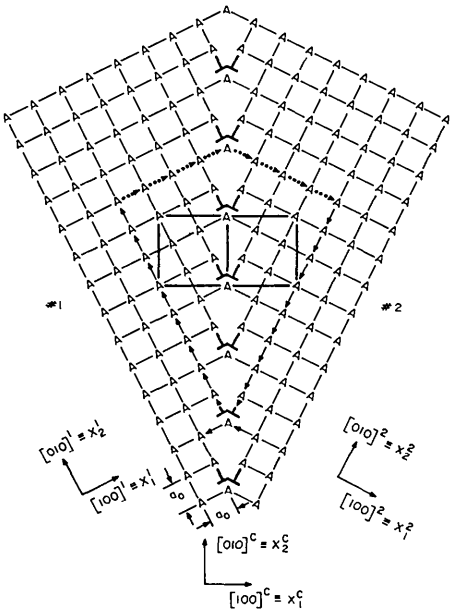

Fig. 7. Burgers circuit about a 53·1° symmetric tilt boundary.

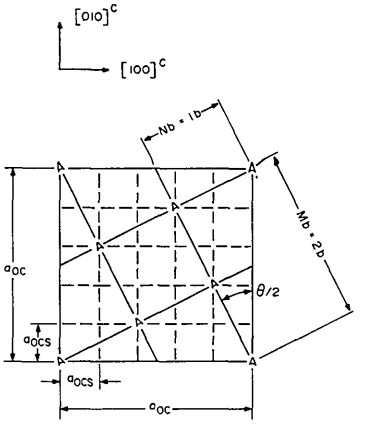

Fig. 8. Coincidence-site-lattice unit cell associated with the 53·1° grain boundary shown in Fig. 7.

The Burgers circuit associated with a high-angle grain boundary

It is intuitively obvious that a simple relationship must exist between the grain-boundary dislocation density $\bar{\boldsymbol{\alpha}}$ given by equation (34) and the Burgers circuit associated with a grain boundary, and was first shown by Bilby (1955). Following Kröner (1958), the total Burgers vector **B** associated with a given Burgers circuit may be written as follows:

$$\left.\begin{aligned} \mathbf{B} &= -\oint_L \mathbf{dLD} = -\int_s \mathbf{ds}\ \mathrm{curl}\ \mathbf{D} \\ B_k &= -\oint_L D\mathrm{d}L_k = -\int_s \varepsilon_{ijk} D_{ij} \mathrm{d}s_i \end{aligned}\right\}, \qquad (48)$$

where the first integral is simply the line integral of the distortion, *i.e.* Burgers circuit, while the second integral is the surface integral taken within the area outlined by the Burgers circuit. The line and surface integrals of equation (48) are clearly connected by Stokes's theorem. From the relation (Kröner, 1958)

$$\mathbf{B} = \int \mathbf{ds} \,.\, \boldsymbol{\alpha} \qquad (49)$$

it follows that

$$\boldsymbol{\alpha} = \mathrm{curl}\ \mathbf{D} \qquad (50)$$

so that the surface integral in equation (48) is simply the total dislocation content within the Burgers loop. Since the dislocation content is concentrated along the plane of the grain boundary, whose normal is **n** within the Burgers loop, we may write (Kröner, 1958)

$$\boldsymbol{\alpha} = \bar{\boldsymbol{\alpha}} \delta(n) \qquad (51)$$

where $\delta(n)$ is a delta function which is zero everywhere except at $n=0$. Since equation (50) could also be written as

$$-\boldsymbol{\alpha} = \mathbf{n} \times (\mathbf{D}_2 - \mathbf{D}_1)\delta(n) \qquad (52)$$

the derivation of equation (34) follows immediately.

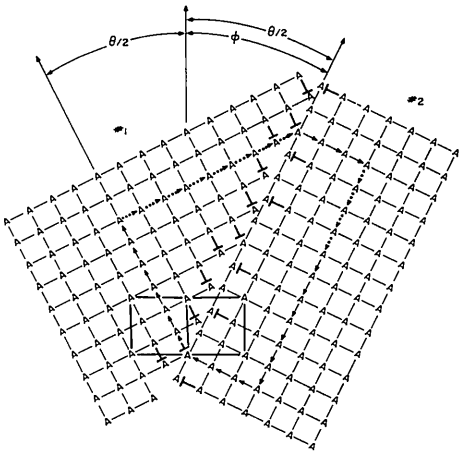

Fig. 9. Straight asymmetric high-angle tilt boundary with $\theta = 53{\cdot}1°$ and $\varphi = 26{\cdot}6°$ in a simple cubic lattice.

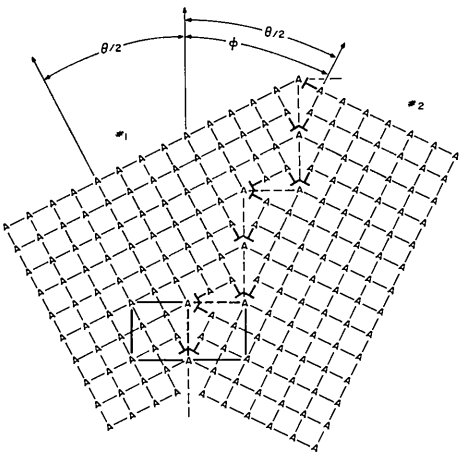

Fig. 10. Stepped asymmetric high-angle tilt boundary with $\theta = 53{\cdot}1°$ and $\varphi = 26{\cdot}6°$ in a simple-cubic lattice.

It is now possible to consider the Burgers circuits associated with the symmetric and asymmetric grain boundaries of Fig. 7 and 9 respectively. In particular, consider interatomic jumps of equal magnitude along equivalent directions in grains #1 and #2 starting and ending on a coincident-site atom *A* located in the boundary. Each atom jump in Figs. 7 and 9 is shown by an arrow. The solid arrows designate equivalent jumps which are present in equal numbers along equivalent directions in grains #1 and #2. The dotted arrows represent the extra jumps, the sum of which is merely the closure failure of the circuit. In other words, the four dotted arrows associated with grains #1 and #2 in Fig. 7, represent the number of extra half planes measured along the x_1 directions of grains #1 and #2. Similarly, in the case of Fig. 9, the group of eight dotted arrows corresponds to the number of extra half planes measured along the x_1 direction of grain #1, while the second group of four dotted arrows represents the number of extra half planes measured along the x_2 direction of grain #2. For the stepped asymmetric grain boundary shown in Fig. 10, a Burgers circuit identical to that shown in Fig. 9 may be constructed, where it will be noted that the closure failures are the same in the two cases. The four-step closure failure may be associated with the four dislocations enclosed by the circuit which possess Burgers vectors in equivalent [010] directions in both grains, while the eight-step closure failure may be associated with the remaining eight dislocations enclosed by the Burgers circuit which have Burgers vectors that lie along the equivalent [100] direction of the two adjacent grains. The dislocation density associated with the stepped boundary of Fig. 10 will of course be lower then that given by the straight boundary of Fig. 9, since the same number of dislocations are spaced over a longer length of boundary. Alternatively, this same result could have been arrived at by the use of equation (34). It will also be noted that whereas

only one coincident-site atom is associated with the Burgers circuit of Fig. 9, the corresponding circuit when made in Fig. 10, contains six coincident-site atoms. Since, as will be shown later, coincidence-site atoms correspond to lower-energy configurations, the stepped grain boundary of Fig. 10 is believed to be of lower energy than the corresponding straight boundary.

Still more subtle and interesting observations can be associated with the Burgers circuits of Figs. 7 and 9 and these are shown in Figs. 11 and 12 respectively. In particular, it is clear that the triangles *EFG* and *CDG* are identical, but differently oriented. In particular, $FE=Nb=CD$, which is simply the component of displacement $u_1^{1,c}$ illustrated in Fig. 5 while $GE=x_2^c=x_2^1$ and $DE=x_2^c-Mb$. The latter quantity is the component of displacement $u_2^{2,c}$ of Fig. 5. It is important to note that in the continuum approximation, the total Burgers-vector components associated with a given grain-boundary circuit can be expressed either as $B_1=FE$ or $B_1=CD$, or as $B_2=FC$ or $B_2=DE$. However, in the crystal lattice, as presented in Figs. 7 and 9, it is only the designations of B_i in terms of *FE* and *FC* that have any physical meaning. The reason for this is apparent when it is realized that it is crystallographically not possible to take the wedge *GFE* in Fig. 11 or Fig. 12 and reinsert it as *GDC* without altering the initial crystallographic description of the grain boundary. Thus, in describing the dislocation density in terms of an ideal reference lattice (Nabarro, 1967; Hirth & Lothe, 1968), *i.e.* either the coincidence-site lattice of Fig. 7 or grain #2 in Fig. 9, it is only the continuum-theory approximation which makes it possible to carry out such a construction. Crystallographically, such a construction is not valid; however, it has been used as the basis of Bollmann's (1970) *O*-lattice formulation of the grain boundary. Finally, for completeness

$$\left.\begin{aligned}\mathbf{B}&=\bar{\boldsymbol{\alpha}}\,.\,(\mathbf{GE}\times\mathbf{n})\\ B_i&=\bar{\alpha}_{ij}\varepsilon_{jkl}(GE)_k n_l\end{aligned}\right\}. \tag{53}$$

Descriptions of the Burgers circuit about a general grain boundary, but with somewhat different emphasis, have previously been carried out by Hirth & Balluffi (1973), Hirth & Lothe (1968) and Marcinkowski & Sadananda (1973). It is to be emphasized at this point that all of the discussion of the present section applies equally well to high as well as to low-angle boundaries.

Interrelationship between grain boundaries with different orders of coincidence

It is next of interest to be able to generate one type of grain boundary from another. An approximate relationship which enables this to be accomplished has already been derived (Marcinkowski & Dwarakadasa, 1973). It is also possible to derive an exact relationship which gives somewhat more insight into the problem. To begin with, if a symmetric tilt boundary with tilt angle θ is changed by θ', the final angle can be written as $\theta+\theta'$ which with the aid of a simple trigonometric identity gives

$$\tan(\theta/2+\theta'/2)=\frac{\tan\theta/2+\tan\theta'/2}{1-\tan\theta/2\tan\theta'/2}\,. \tag{54}$$

The $\tan\theta/2$ function is readily obtained from equation (46). On the other hand, $\tan\theta'/2$ can be obtained from the following relationship

$$\tan\theta'/2=\frac{N'b_s}{M'b_s}=\frac{N'}{M'} \tag{55}$$

where b_s is the Burgers vector corresponding to the magnitude of the unit cell edge length a_{0cs} in much the same way as b was connected to a_0. Reference to Fig. 8, which was drawn for the 53·1° grain boundary, shows that a_{0cs} is simply the unit-cell edge length associated with the sublattice of the coincidence-site lattice corresponding to θ. In general

$$a_{0cs}=\frac{a_{0c}}{(N^2+M^2)}\,. \tag{56}$$

The quantity a_{0cs} in turn may also be related to a_0 by

$$a_0=a_{0cs}(N^2+M^2)^{1/2} \tag{57}$$

which is similar in form to equation (47). It can thus be concluded that all of the tensor quantities associated with the distortion that gave rise to θ can now be ap-

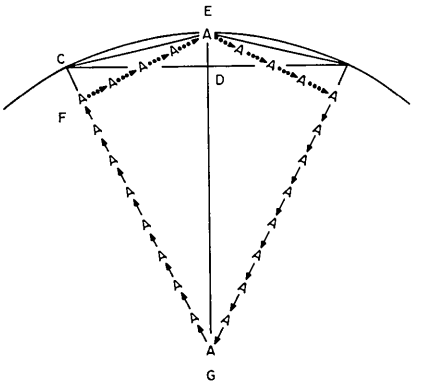

Fig. 11. Elaboration of the Burgers circuit shown in Fig. 7.

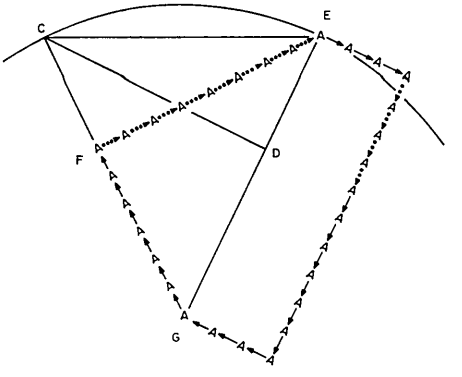

Fig. 12. Elaboration of the Burgers circuit shown in Fig. 9.

plied to the distortion that changes θ to θ'. However, whereas in the former case the crystal-lattice unit cell was used to determine the unit of plastic deformation, it now becomes the sublattice unit cell of the coincidence-site lattice corresponding to θ.

The quantity $N'b_s$ in the numerator of equation (55) may be written either as

$$N'_1 b_s = N'_1 b_1(\cos\theta/2)/M = b_{1,c} \qquad (58a)$$

or

$$N'_2 b_s = N'_2 b_2(\sin\theta/2)/N = b_{2,c} \qquad (58b)$$

where $|b_1|=|b_2|=|a_0|$, $|b_{1\,c}|=|b_{2\,c}|=|a_{0cs}|$ and where the common 1 or 2 subscript in either of the above relations is used to denote the fact that the Burgers vector corresponding to the particular dislocation lies along either the x_1^c or x_2^c direction respectively. The quantity $M'b_s$ in the denominator of equation (55) measures the spacing between the offsets of magnitude $N'b_s$ in terms of the coincidence-site-lattice unit-cell sublattice. Specifically, when equation (58*a*) is valid

$$M'_2 b_s = M''_2 a_{0c} - N'_2 b_s \qquad (59a)$$

while in case of equation (58*b*)

$$M'_2 b_s = M''_2 a_{0c} - N'_2 b_s\,. \qquad (59b)$$

With these considerations in mind, equation (54) can be reduced to

$$\tan\left(\frac{\theta+\theta'}{2}\right) = \frac{NM'+N'M}{MM'-NN'}\,. \qquad (60)$$

As an example of the use of the above relations, Fig. 13 shows the creation of a 53·1° grain boundary from a 36·9° boundary. Inspection of the figure shows that $N=1$, $M=3$, $N'=N'_2=1$ and $M'=M'_1=7$. In addition $M''_1=1$ and $N'_1=3$, which leads to

$$\tan\left(\frac{\theta+\theta'}{2}\right) = \tfrac{1}{2} = \frac{N}{M} = \tan\left(\frac{53{\cdot}1}{2}\right)\,. \qquad (61)$$

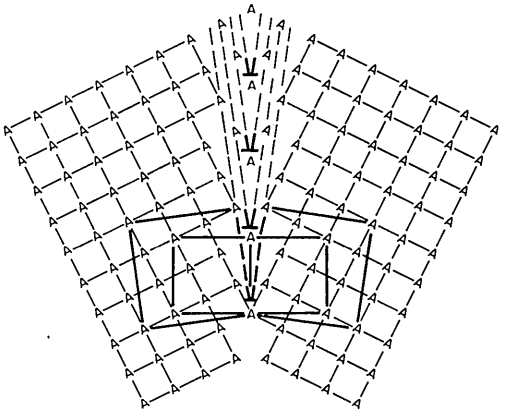

Fig. 13. Generation of a 53·1° grain boundary from a 36·9° boundary.

The extra half planes derived from the 36·9° coincidence-site lattice are outlined by dashed lines in Fig. 13, and from equation (58) are readily seen to be of strength $b_s = b\sin(36{\cdot}9/2)$. It is also important to note that the quantity $M'b_s$ in equation (55) also corresponds to the unit cell edge length a'_{0c} of the new coincidence-site lattice corresponding to θ'.

The quantities given in equation (58) also form the basis of the following relationship:

$$\mathbf{b}_{GB} = \mathbf{b}_{CL}^{\#1} + \mathbf{b}_{CL}^{\#2} \qquad (62)$$

where $\mathbf{b}_{CL}^{\#1}$ and $\mathbf{b}_{CL}^{\#2}$ correspond to the crystal lattice dislocations in grains $\#1$ and $\#2$ which have come together at the grain boundary to give the grain boundary dislocation $\mathbf{b}_{GB}$ of strength twice that given by equation (58). More specifically, equation (62) may be viewed as the dislocation reaction which occurs at every coincident-site lattice point lying within a symmetric grain boundary, as can be seen in Figs. 7, 10 and 13. Equation (62) also provides justification for the conclusion that all symmetric grain boundaries can be described in terms of combinations of equal numbers of crystal lattice dislocations from the two adjacent grains (Marcinkowski, Sadananda & Tseng, 1973).

High-angle boundaries in arbitrary crystal structures

The procedures discussed in the previous sections with respect to simple cubic crystals can readily be extended to arbitrary crystals. This is most conveniently demonstrated by considering grain boundaries in a body-centered cubic crystal (Marcinkowski, Tseng & Dwarakadasa, 1974). As an example, Fig. 14 shows a 70·5° twist boundary in a body-centered cubic crystal which terminates on a symmetric tilt boundary. Both the edge-type and screw-type grain-boundary dislocations are shown in heavy outline and may be visualized as being derived from a relationship of the type given by equation (62). Note also that the two sets of grain-boundary dislocations associated with the twist boundary in Fig. 14 outline a coincidence-site-lattice unit cell which is shown in more detail in Fig. 15. It is thus possible to write a somewhat more generalized version of the coincidence-site-lattice relationship given by equation (46) as follows:

$$\tan\theta/2 = \frac{Nb_1}{Md_2} \qquad (63)$$

where b_1 is the component of the Burgers vector of the crystal lattice dislocation resolved along the x_1 axis of either grain, while d_2 is the interplanar spacing between planes on which these dislocations lie. The quantity b_1 in equation (63) may be expressed follows:

$$b_1 = \frac{\sqrt{3}a_0}{2}\,\frac{Hh+Kk+Ll}{(H^2+K^2+L^2)^{1/2}(h^2+k^2+l^2)^{1/2}} \qquad (64)$$

where h,k,l are indices associated with the direction of the Burgers vector, while H,K,L are indices associated

with the x_1 direction in the grain of interest. The interplanar spacing d_2 may be written as

$$d_2 = \frac{a_0}{(h_p^2 + k_p^2 + l_p^2)^{1/2}} \tag{65}$$

where the indices h_p, k_p, l_p pertain to the plane upon which the dislocation lies. Equations (63), (64) and (65) can be combined to give

$$\tan\frac{\theta}{2} = \frac{N}{M}\frac{\sqrt{3}}{2}(h_p^2 + k_p^2 + l_p^2)^{1/2} \times \left[\frac{Hh + Kk + Ll}{(H^2 + K^2 + L^2)^{1/2}(h^2 + k^2 + l^2)^{1/2}}\right]. \tag{66}$$

In Fig. 14 the values of H, K, L are $0, 0, \bar{1}$ while h, k, l are $1, 1, \bar{1}$ and h_p, k_p, l_p are $\bar{1}, 1, 0$ so that equation (66) becomes

$$\tan\theta/2 = \frac{N}{M}\frac{\sqrt{2}}{2}. \tag{67}$$

For the specific boundary shown in Fig. 14, $N = 1$ and $M = 1$, while $b_1 = a_0/2$ and $d_2 = \sqrt{2}a_0/2$, giving a value of $\theta = 70{\cdot}5°$.

Close inspection of Figs. 14 and 15 shows that a coincidence-site-lattice unit cell has been chosen which is a true unit cell only with respect to the projection of atoms along the [110] direction. The true coincidence-site-lattice unit cell has a value of a_{0c} twice that shown in Fig. 15; however, because of convenience, the smaller unit cell will be used. Another important point to note in constructing a generalized grain boundary is that the crystal lattice dislocations associated with the two adjacent grains must be chosen such that their resultant Burgers vector lies along the common x_1^c direction. All other components must vanish. Thus, in the case of Fig. 14, the crystal lattice dislocations from grain #1 comprising the grain boundary possess a Burgers vector given by $\frac{1}{2}a_0[11\bar{1}]$ while those from grain #2 possess values of $\frac{1}{2}a_0[11\bar{1}]$. Once again, just as it was possible to relate all tensor quantities to the distortions given in terms of the coincident-site-lattice unit-cell sublattice, it now also becomes possible to relate these same quantities to those defined in equation (63) for arbitrary crystals and similarly to their respective sublattices.

The unit-cell edge lengths a_{0c} and b_{0c} in Fig. 15 can be expressed in vector notation as follows:

$$\mathbf{b}_{0c} = N\mathbf{b}_1 + M\mathbf{d}_2 \tag{68a}$$

$$\mathbf{a}_{0c} = N'\mathbf{b}_1 - M'\mathbf{d}_2 \tag{68b}$$

where the primed integers do not have the same physical meaning defined earlier. It is also apparent that the coincident-site-lattice unit-cell edge lengths similar to equation (47) are given by $\mathbf{b}_{0c} \cdot \mathbf{b}_{0c}$ and $\mathbf{a}_{0c} \cdot \mathbf{a}_{0c}$. Furthermore, since $\mathbf{b}_{0c} \cdot \mathbf{a}_{0c} = 0$, it follows from equations (68) that

$$\left(\frac{b_1}{d_2}\right)^2 = \frac{MM'}{NN'}, \tag{69}$$

so that the choice of the four integers is constrained by the above relation. In addition, the number of atoms within the coincidence-site-lattice unit cell is given by

$$n = \frac{a_{0c}b_{0c}}{b_1 d_2}. \tag{70}$$

Thus, the smaller the value of n, the greater the number of atoms on coincidence sites, and since these represent low-energy configurations, the lower the corresponding energy. Equations (68), (69), and (70) can be utilized to give

$$n = \left[\frac{N'M'M}{N} + (M')^2\right]^{1/2}\left[(N)^2 + \frac{MNN'}{M'}\right]^{1/2}. \tag{71}$$

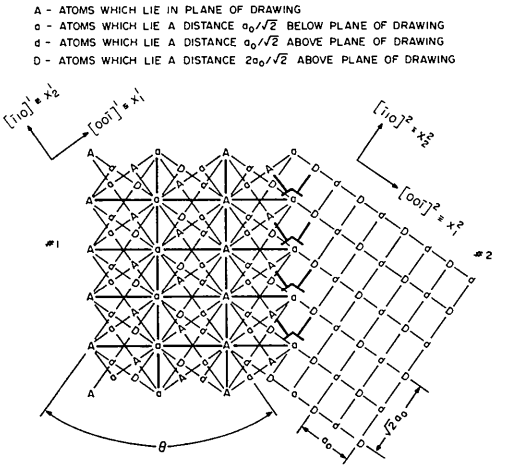

Fig. 14. Termination of a high-angle twist boundary of misorientation angle 70·5° on a symmetric tilt boundary in a body-centered cubic lattice. Rotation axis is [110] and is normal to drawing.

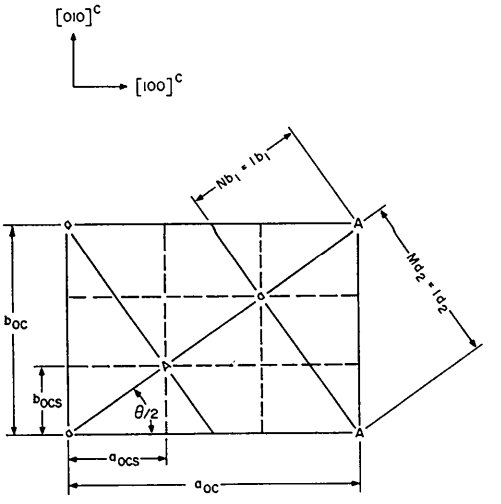

Fig. 15. Coincidence-site-lattice unit cell associated with the 70·5° grain boundary shown in Fig. 14.

It is also easy to see that the coincidence-site-lattice unit cell sublattice unit vectors are given by

$$\mathbf{b}_{0cs}=\frac{\mathbf{a}_{0c}}{n} \tag{72a}$$

and

$$\mathbf{a}_{0cs}=\frac{\mathbf{b}_{0c}}{n}. \tag{72b}$$

For the specific case shown in Fig. 15, $N=1$, $M=1$, $N'=2$ and $M'=1$ so that from equation (71), $n=3$, as can be verified by inspection of this figure. It is also apparent that equation (71) could have also been used in connection with the simple-cubic system discussed earlier.

It is important to note the role played by crystal symmetry in the present analysis. For example, in the case of the simple-cubic crystal of Fig. 7, a rotation of the two adjacent grains by 90° instead of 53·1° would again generate a perfect crystal. On the other hand, the various tensor quantities associated with such a boundary would still have finite values. This is simply a reflection of the fact that the description of grain boundaries in terms of a distortion tensor reflects the history of the way the boundary was constructed from an initially perfect crystal. Thus, it is expected that certain distortions may regenerate a new perfect crystal, but such operations are trivial and under these conditions the crystal should obviously be viewed as possessing no grain boundaries and thus no grain boundary dislocations.

There are also certain symmetries associated with twist boundaries with a [001] rotation axis (Marcinkowski & Dwarakadasa, 1973). In particular, such boundaries with rotation angles of 53·1° and 36·9° are identical, or more generally, those twist boundaries with $\pi/2-\theta$ and θ are equivalent, where θ is any coincidence lattice angle.

Finally, the individual Burgers vectors associated with the grain boundaries in the present analysis may not be unique, especially in the case of twist boundaries where interactions may take place between the two sets of screw dislocations. However, each grain boundary may be viewed as generated by means of a well-defined distortion, *i.e.* unique set of dislocations, so that whatever the final arrangement of this set of dislocations, the closure failure, which measures the net dislocation content of such a boundary, must also be unique.

Summary and conclusions

The coincident-site-lattice theory of grain boundaries has been shown to be compatible with those concepts embodied in the continuum theory of dislocations. In particular, such quantities as the distortion tensor, grain-boundary dislocation-density tensor and incompatibility tensor are all developed in a rather straightforward manner around the concept of a coincident-site lattice. Furthermore, the Burgers circuit associated with a grain boundary is shown to be a straightforward extension utilizing the above ideas. The methods can be applied to grain boundaries within any given crystal structure. In addition, the treatment is sufficiently general so as to be readily extended to two-phase interfaces by including non-zero diagonal elements in the distortion tensor. One of the limitations of the present analysis is that all of the grain boundaries have been described in terms of a rigid medium, with no relaxation being allowed at the boundary. Further refinements and extensions of the present theory will be treated in more detail in subsequent studies.

The authors would like to express their thanks to Dr R. de Wit of The Metallurgy Division and Institute for Materials Research of The National Bureau of Standards, Washington, D. C., for a number of stimulating discussions dealing with dislocation theory. Financial support for the present study was provided by The National Science Foundation under Grant No. GH-32262.

References

BILBY, B. A. (1955). *Report of The Conference on Defects in Crystalline Solids, The University of Bristol, July* 1954, pp. 124–133. London: The Physical Society.

BOLLMANN, W. (1970). *Crystal Defects and Crystalline Interfaces*. Berlin: Springer-Verlag.

COTTRELL, A. H. (1957). *Dislocations and Mechanical Properties of Crystals*, edited by J. C. FISHER, W. G. JOHNSTON, R. THOMSON and T. VREELAND JR, p. 509. New York: John Wiley.

DAS, E. S. P. & MARCINKOWSKI, M. J. (1971*a*). *J. Mater. Sci. Eng.* **8**, 189–197.

DAS, E. S. P. & MARCINKOWSKI, M. J. (1971*b*). *J. Appl. Phys.* **42**, 4107–4109.

DAS, E. S. P. & MARCINKOWSKI, M. J. (1972). *Acta Met.* **20**, 199–206.

DUSCHEK, A. & HOCHRAINER, A. (1960). *Grundzüge der Tensorrechnung in Analytischer Darstellung*. Vienna: Springer-Verlag.

FLÜGGE, W. (1972). *Tensor Analysis and Continuum Mechanics*. New York: Springer-Verlag.

FUNG, Y. C. (1965). *Foundations of Solid Mechanics*. New York: Prentice–Hall.

HIRTH, J. P. & BALLUFFI, R. W. (1973). *Acta Met.* **21**, 929–942.

HIRTH, J. P. & LOTHE, J. (1968). *Theory of Dislocations*. New York: McGraw-Hill.

KRÖNER, E. (1958). *Kontinuumstheorie der Versetzungen und Eigenspannungen*, Berlin: Springer-Verlag.

KRÖNER, E. (1966). *Theory of Crystal Defects*, Edited by B. GRUBER, p. 231. New York: Academic Press.

MARCINKOWSKI, M. J. (1970). *Fundamental Aspects of Dislocation Theory*, NBS Special Publication No. 317, Edited by J. A. SIMMONS, R. DE WIT and R. BULLOUGH, pp. 531–545.

MARCINKOWSKI, M. J. (1972). *Electron Microscopy and Structure of Materials*, Edited by G. THOMAS, R. M. FULRATH and R. M. FISHER, pp. 382–416. Berkeley: Univ. of California Press.

MARCINKOWSKI, M. J. & DAS, E. S. P. (1972). *Phil. Mag.* **26**, 1281–1300.
MARCINKOWSKI, M. J., DAS, E. S. P. & SADANANDA, K. (1973). *Phys. Stat. Sol.* (*a*) **19**, 67–81.
MARCINKOWSKI, M. J. & DWARAKADASA, E. S. (1973). *Phys. Stat. Sol.* (*a*) **19**, 597–608.
MARCINKOWSKI, M. J. & SADANANDA, K. (1973). *Phys. Stat. Sol.* (*a*) **18**, 361–375.
MARCINKOWSKI, M. J., SADANANDA, K. & TSENG, W. F. (1973). *Phys. Stat. Sol.* (*a*) **17**, 432–433.
MARCINKOWSKI, M. J. & TSENG, W. F. (1970). *Metallurg. Trans.* **1**, 3397–3401.
MARCINKOWSKI, M. J., TSENG, W. F. & DWARAKADASA, E. S. (1974). *J. Mater. Sci.* **9**, 29–40.
NABARRO, F. R. N. (1967). *Theory of Crystal Dislocations.* Oxford: Clarendon Press.
NYE, J. F. (1957). *Physical Properties of Crystals.* Oxford: Clarendon Press.
SADANANDA, K. & MARCINKOWSKI, M. J. (1973). *Scripta Met.* **7**, 557–564.
SADANANDA, K. & MARCINKOWSKI, M. J. (1974*a*). *J. Mater. Sci.* **9**, 245–257.
SADANANDA, K. & MARCINKOWSKI, M. J. (1974*b*). *J. Appl. Phys.* **45**, 1533–1543.
SADANANDA, K. & MARCINKOWSKI, M. J. (1974*c*). *J. Appl. Phys.* **45**, 1521–1532.
TSENG, W. F., MARCINKOWSKI, M. J. & DWARAKADASA, E. S. (1974). *J. Mater. Sci.* **9**, 41–56.
WIT, R. DE (1970). *Fundamental Aspects of Dislocation Theory.* NBS Special Publication No. 317, Edited by J. A. SIMMONS, R. DE WIT and BULLOUGH, Vol. 1. pp. 651–673.

Acta Cryst. (1975). A**31**, 292

Theory of Simple Two-Phase Interfaces*

BY M. J. MARCINKOWSKI,† K. SADANANDA AND W. H. CULLEN JR‡

Engineering Materials Group and Department of Mechanical Engineering, University of Maryland, College Park, Maryland 20742, *U.S.A.*

(*Received* 4 *September* 1974; *accepted* 10 *January* 1975)

The coincidence-site-lattice theory of grain boundaries has been applied to simple two-phase boundaries. Symmetric and unsymmetric tilt boundaries, pure twist boundaries and unrotated and untwisted boundaries have all been considered. It has been shown that each type of boundary can be described in terms of a characteristic coincidence-site lattice. In addition, the dislocation content within the interphase boundaries has been defined in terms of Burgers circuits described with respect to the original crystal lattices in the new coincidence-site lattices.

Introduction

It was first proposed that a coherent boundary between two phases of differing lattice constant could be described in terms of interface dislocations (Marcinkowski, 1970*a*). Those interface dislocations were originally referred to as virtual dislocations, since they appeared then to be fundamentally different from crystal-lattice dislocations. The subsequent development of the coincidence-site-lattice theory of grain boundaries however showed this not to be the case (Marcinkowski & Sadananda, 1973).

Although a number of preliminary treatments of interface dislocations have been presented (Marcinkowski, 1970*a*,*b*; Marcinkowski & Tseng, 1970; Marcinkowski, 1972; Sadananda & Marcinkowski, 1974*a*; Cullen, Marcinkowski & Das, 1973), none has yet been extensive. It is the purpose of the present effort to carry out the first of such studies. The presentation will be pedagogic in nature, relying heavily on simple geometric models. A fuller mathematical analysis will follow in a subsequent publication (Marcinkowski & Kröner, 1975). The analysis will be confined to what is perhaps the simplest of all two-phase boundaries in which the two phases A and B possess the same simple cubic structures but have differing interplanar spacings a_0 and b_0 such as shown in Fig. 1(*a*). The two-phase interface may be visualized as comprised of a parallel array of edge-type interface dislocations (shown dotted) associated with each interatomic spacing in which the Burgers vector of each interface dislocation is given by

$$|\mathbf{b}_{IB}| = a_0 - b_0. \qquad (1)$$

For the particular case shown in Fig. 1(*a*), $b_0 = \frac{9}{10}a_0$.

It is apparent that the array of interface dislocations shown in Fig. 1(*a*) generate long-range stresses In order that these stresses be reduced, an array of edge-type crystal-lattice dislocations of strength $|\mathbf{b}_{CL}| = b_0$ can be introduced into the boundary as shown by the solid dislocation symbols in Fig. 1(*b*). It is a simple matter to show that the long-range stresses are fully compensated when the spacing between the crystal-

* The present research effort was supported by The National Science Foundation under Grant No. GH-32262.

† Presently on sabbatical leave at Institut für Theoretische und Angewandte Physik der Universität Stuttgart, Germany (BRD).

‡ Now with the U. S. Naval Research Laboratory, Washington, D. C. 20390.